Available online at www.sciencedirect.com
ScienceDirect
Journal of Power Sources 172 (2007) 1007–1011
JOURNAL OF POWER SOURCES
www.elsevier.com/locate/jpowsour

Short communication

Supercapacitive behaviors and their temperature dependence of sol–gel synthesized nanostructured manganese dioxide in lithium hydroxide electrolyte

Xiuling Wang, Anbao Yuan *, Yuqin Wang

Department of Chemistry, College of Sciences, Shanghai University, Shanghai 200444, PR China

Received 4 June 2007; received in revised form 9 July 2007; accepted 31 July 2007
Available online 6 August 2007

Abstract

In the present work, a nanostructured manganese dioxide material was synthesized by a sol–gel method starting with manganese acetate ($MnAc_2{\cdot}4H_2O$) and citric acid ($C_6H_8O_7{\cdot}H_2O$) raw materials, and characterized by X-ray diffraction, infrared spectroscopic and transmission electron microscope techniques. The electrochemical properties and the influence of temperature on supercapacitive behaviors of the nano-MnO_2 electrode in 1 M LiOH electrolyte were investigated using electrochemical methods. Experimental results show that the MnO_2 electrode can exhibit an excellent pseudocapacitive behavior in 1 M LiOH electrolyte, and a high specific capacitance of 317 F g^{-1} can be obtained at a charge/discharge current rate of 100 mA g^{-1} and at the temperature of 25 °C. We found that temperature has a crucial influence on the discharge specific capacitance of the electrode. The specific capacitance at 25 °C is higher than that at 15 or 35 °C.

Keywords: Nanostructured manganese dioxide; Sol–gel synthesis; Pseudocapacitive behavior; Temperature dependence; Lithium hydroxide electrolyte

1. Introduction

Electrochemical supercapacitors have attracted great attentions since 90s in the passed century. As charge storage devices, supercapacitors can be used in many fields such as hybrid electric vehicles and electrical equipments [1,2]. For the developments and applications of supercapacitors, electrochemical system and electrode materials are important considerations in respect to energy and power densities. Although, hydrous ruthenium oxide ($RuO_2{\cdot}nH_2O$) has been reported to exhibit a high capacitance of 760 F g^{-1} and an excellent cyclability in sulfuric acid medium [3], but it is considered too expensive to be commercially attractive. Hence, other metal oxides with lower cost have been also studied as electrode materials for supercapacitors, such as NiO, Co_3O_4, V_2O_5, Fe_3O_4, Bi_2O_3, In_2O_3, SnO_2, and MnO_2, etc [4–11]. Among various metal oxides, the nanostructured MnO_2 has the advantages of large specific area, wider charge/discharge potential range, higher specific faradic redox pseudocapacitance, low cost and good environmental compatibility. Since the first report of amorphous hydrous $MnO_2{\cdot}nH_2O$ as supercapacitor material in mild KCl aqueous electrolyte in 1999 [11], MnO_2 becomes an attractive material for electrochemical capacitors [12–27]. In these studies, various mild aqueous solutions were used as electrolytes, and corrosion-resistance metals such as titanium, stainless steel or gold was employed as current collector in consideration of current collector corrosion in these electrolytes caused by electro-oxidation upon charging process.

Alternatively, a nanostructured manganese dioxide/activated carbon hybrid supercapacitor using 1 M LiOH alkaline aqueous solution as electrolyte and foamed nickel as current collector was reported in the prior work recently [28], in which the charge storage mechanism of the MnO_2 electrode was suggested to be associated with a reversible insertion/extraction of Li^+ ions in MnO_2 accompanied by charge transfer at the electrode/electrolyte interface, providing a considerable pseudocapacitance contribution. In fact, we found from comparative study that for a given nanostructured MnO_2 material, the specific capacitance and rate charge/discharge ability of the MnO_2 electrode in LiOH electrolyte is much superior to that in mild aqueous electrolytes such as Na_2SO_4, K_2SO_4 and KCl solutions,

* Corresponding author. Tel.: +86 21 66134851; fax: +86 21 66132797.
E-mail address: abyuan@shu.edu.cn (A. Yuan).

0378-7753/$ – see front matter © 2007 Elsevier B.V. All rights reserved.
doi:10.1016/j.jpowsour.2007.07.066

etc. In the prior work, the nanostructured manganese dioxide was prepared by a solid-reaction route. To our knowledge, the electrochemical properties of a manganese dioxide are correlated with its preparation and structure. In this work, a nanostructured manganese dioxide material was synthesized by a sol–gel technique and was investigated as a supercapacitor electrode in 1 M LiOH electrolyte. The specific capacitance of the present MnO_2 was found to be much superior to that of the prior work. In addition, the influence of temperature on supercapacitive behaviors of the nano-MnO_2 electrode in 1 M LiOH electrolyte is reported here for the first time.

2. Experimental

2.1. Preparation of nanostructured manganese dioxide material

Manganese acetate ($MnAc_2{\cdot}4H_2O$) and citric acid ($C_6H_8O_7{\cdot}H_2O$) with a mol ratio 1:2 were dissolved in distilled water in a beaker. The solution was adjusted to pH 6 by addition of ammonia. Then, the solution was heated to 80 °C with a magnetic stirring and kept this temperature for several hours until a wet gel was obtained. The wet gel was dried at 110 °C in a drying box, and a dried gel was obtained. Then the dried gel was calcined at 380 °C for 12 h in a muffle furnace. The calcined product was acid-treated in 2 M H_2SO_4 solution for 2 h at 80 °C with a magnetic stirring in order to increase the degree of oxidation of the product. After acid-treatment, the product was rinsed with distilled water and filtrated, then dried at 105 °C, and finally the brownish black manganese dioxide material was obtained.

2.2. Characterization of nanostructured manganese dioxide material

The prepared manganese dioxide material was characterized by X-ray diffraction (XRD) and infrared spectroscopic (IR) analysis as well as transmission electron microscope (TEM) observation. XRD analysis was conducted on a Rigaku D/max-2000 X-ray diffractometer with Cu Kα radiation (40 kV/250 mA, scan rate 0.02° s^{-1}). IR analysis was carried out using a Nicolet Avatar 370 FT-IR Fourier transformation infrared spectrometer (KBr pelleting). TEM observation was performed on a JEOL JEM-200CX transmission electron microscope.

2.3. Fabrication and testing of nanostructured manganese dioxide electrode

Manganese dioxide electrode was fabricated by mixing nanostructured manganese dioxide active material, acetylene black conductor and polytetrafluoroethylene binder (emulsion) with a mass ratio 80:15:5 to form slurry. The slurry was filled into a foamed nickel with an apparent area of 1 cm × 1 cm, and then dried and rolled to a sheet. The loaded mass of nano-MnO_2 in the composite electrode is ca. 0.04 g.

Electrochemical tests for the nano-MnO_2 electrode were conducted using a three-electrode system in which MnO_2 electrode, activated carbon electrode and Hg/HgO (1 M LiOH) electrode were served as working, counter and reference electrodes, respectively, and 1 M LiOH aqueous solution as electrolyte. Cyclic voltammetry and AC impedance measurements were carried out on a Solartron 1287 electrochemical interface coupled with a 1255B frequency response analyzer. Galvanostatic charge/discharge tests were performed on a LAND auto-cycler (China).

3. Results and discussion

3.1. Structural characterization and morphological observation of nanostructured manganese dioxide material

Fig. 1 shows X-ray diffraction (XRD) pattern of the MnO_2 sample. The pattern is similar to that of a typical commercial electrolytic manganese dioxide (EMD) and the γ-MnO_2 reported in the literature [29]. The diffraction peaks occurred at 21.88°, 37.16°, 42.50°, 55.96° and 67.30°, respectively should be assigned to the characteristic peaks for γ-MnO_2 (refer to PDF No. 14-0644). Except for these characteristic peaks, no additional peaks could be observed, indicating the pure phase of γ-MnO_2. The visible broad peaks and unsmooth basal of the diffraction pattern suggest that the material may possess a nanostructure with some amorphous nature.

Fig. 2 shows the infrared spectrum (IR) of the MnO_2 sample. Several absorption bands can be observed at 3445, 1637, 1400, 1107, 566 and 530 cm^{-1}, respectively. The 3445 cm^{-1} band should be attributed to the O–H stretching vibration, and the 1637, 1400 and 1107 cm^{-1} bands are usually attributed to the O–H bending vibrations combined with Mn atoms. While the 566 and 530 cm^{-1} bands should be ascribed to the Mn–O vibrations in MnO_6 octahedra [30]. The IR result suggests the presence of somewhat bound water in the MnO_2 structure, which is generally believed to be favorable to the electrochemical activity of the material.

Fig. 3 shows the transmission electron microscope (TEM) image of the MnO_2 sample. It can be seen from Fig. 3 that

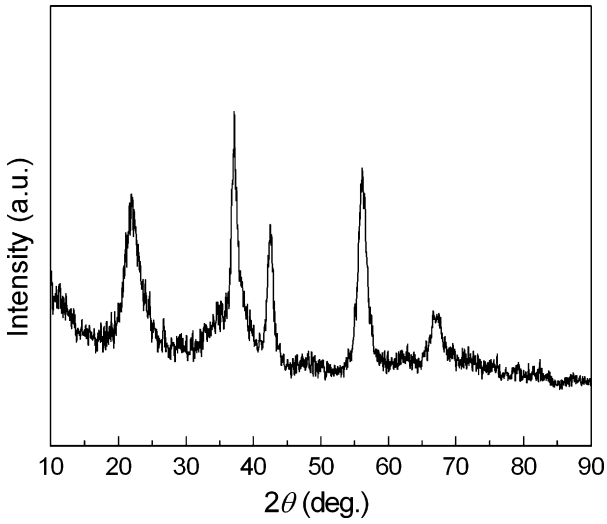

Fig. 1. XRD pattern of the sample.

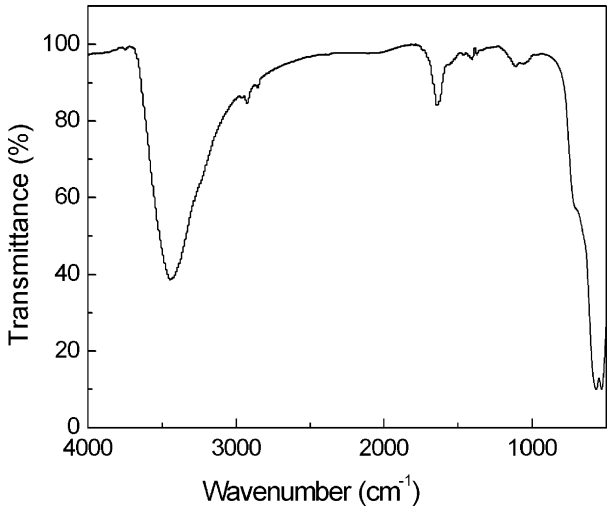

Fig. 2. FT-IR spectrum of the sample.

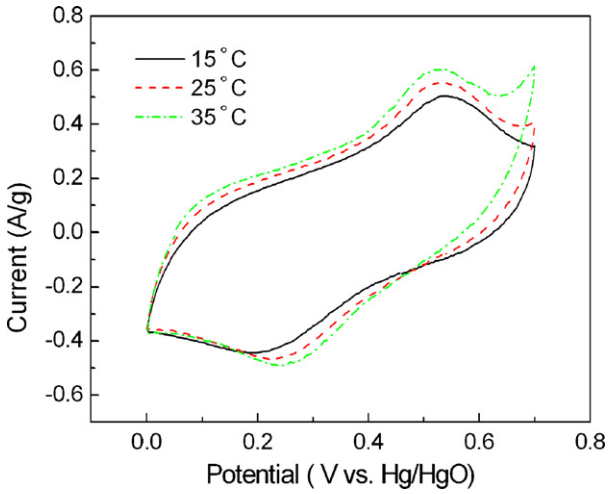

Fig. 4. Temperature dependence of cyclic voltammograph of the MnO_2 electrode in 1 M LiOH solution.

the material is composed of needle-like nanorods with a diameter ranging from several to about ten nanometers and a length ranging from tens to about one hundred nanometers.

3.2. Cyclic voltammetrical and galvanostatic charge/discharge characteristics of nanostructured manganese dioxide electrode

Fig. 4 shows the temperature dependence of cyclic voltammograph of the MnO_2 electrode in 1 M LiOH electrolyte at a scan rate of 1 mV s^{-1}. At any temperature, an obvious redox couple can be observed in the applied potential range of 0–0.7 V (versus Hg/HgO). The anodic and cathodic current peaks are occurred at ca. 0.52 and 0.22 V, respectively. This is similar to the observations in our previous work [28], but the current responses here are larger than that observed in the prior work, suggesting a larger specific capacitance of the present material. This is likely due to the microstructure of the present material. In the prior work, the material is nanograins of mixture of γ-MnO_2 and α-MnO_2 with a diameter less than 100 nm, while, the present material is quasi-one-dimension nanorods of γ-MnO_2 with a diameter less than 10 nm. The small size in the diameter–dimension and the pure phase of γ-MnO_2 may favor the electrochemical redox reaction of the electrode. The redox reaction was suggested to be Li^+ ions insertion/extraction in solid MnO_2 with charge transfer process at the electrode/electrolyte interface, providing a considerable pseudocapacitive contribution [28]. Comparing the three cyclic voltammographs at different temperatures, it can be found that with temperature increasing, the redox peak currents increase, and the anodic and cathodic peak potentials shift toward negative and positive, respectively. This suggests that increase of temperature is favorable to the redox reaction. In addition, with temperature increasing, the onset potential of oxygen evolution decreases, and the observed peak current at 0.7 V increases, especially in the case of 35 °C. This result suggests that increase of temperature can make the oxygen evolution reaction facile.

The galvanostatic charge/discharge profile of the MnO_2 electrode in 1 M LiOH solution at 25 °C is presented in Fig. 5. The charge/discharge current rate is 1000 mA g^{-1} and the operational potential range is between 0 and 1 V (versus Hg/HgO). It can be seen that the charge profile is slightly curved, suggesting a pseudocapacitive characteristic. At the moment of electric

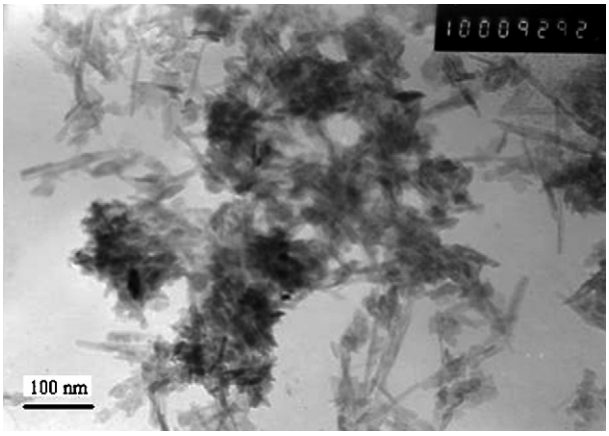

Fig. 3. TEM image of the sample.

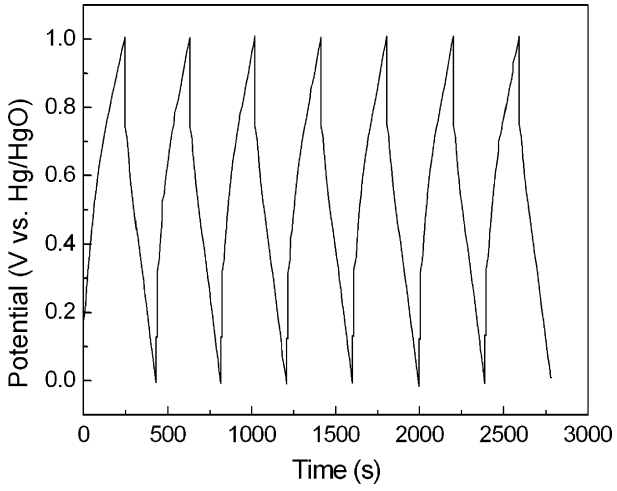

Fig. 5. Charge/discharge profile of the MnO_2 electrode in 1 M LiOH solution.

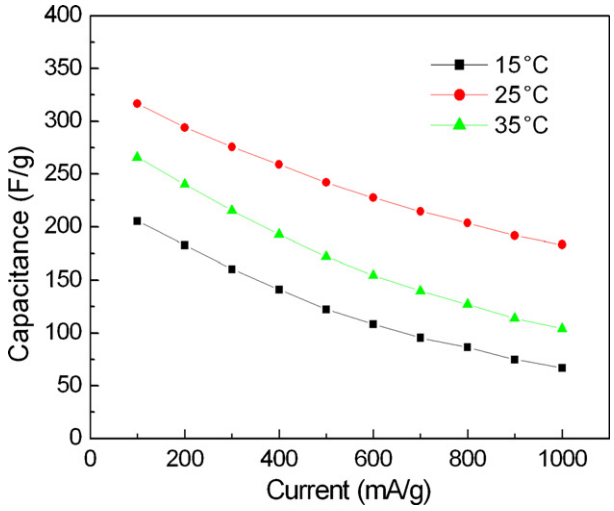

Fig. 6. Discharge specific capacitance vs. current rate for the MnO_2 electrode at different temperatures.

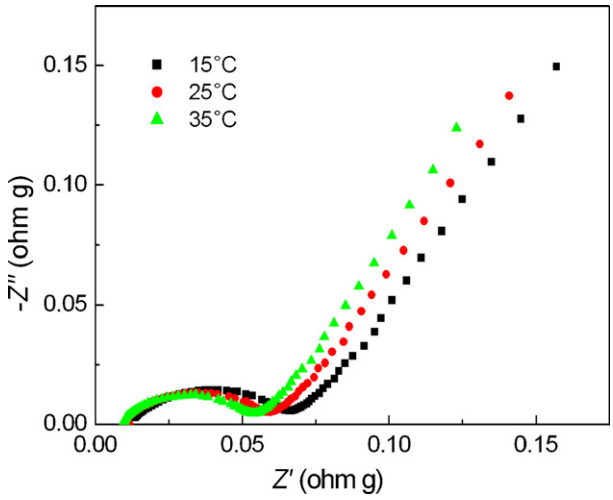

Fig. 7. Temperature dependence of AC impedance of the MnO_2 electrode.

current reversing from charging to discharging, a potential drop can be observed due to the electrode polarization at this high current rate. Except for the initial potential drop, the discharge profile is essentially linear. Actually, when the current rate is not so high, for example, at 100 mA g^{-1}, the potential drop is very small. According to the formula $C_s = It/m\Delta E$ (where, the C_s is the specific capacitance, I is the applied current, t is the discharge time, m is the mass of the active material, and ΔE is the applied potential range), the average discharge specific capacitance of the MnO_2 electrode in the operational potential range can be estimated to be ca. 184 F g^{-1} at this high charge/discharge current rate.

3.3. Influence of temperature on electrochemical properties of nanostructured manganese dioxide electrode

Fig. 6 shows the temperature dependence of discharge specific capacitance of the MnO_2 electrode versus charge/discharge current rate. Firstly, we can see that the discharge specific capacitance of the electrode decreases with charge/discharge current increasing at all the temperatures. This is because that the polarization of the electrode increases with current rate increasing, and hence the specific capacitance decreases with current increasing. Secondly, at the same current rate, when temperature increased from 15 to 25 °C, the specific capacitance increased considerably, suggesting that temperature has a crucial influence on the specific capacitance. However, when temperature further increased from 25 to 35 °C, the specific capacitance decreased. At the temperature of 25 °C, a maximal specific capacitance of 317 F g^{-1} can be obtained at a current rate of 100 mA g^{-1}, and a specific capacitance of 184 F g^{-1} can be obtained even at a high current rate of 1000 mA g^{-1}. As far as powdered electrode is concerned, this electrode can exhibit higher specific capacitance and better rate charge/discharge ability.

In order to interpret the specific capacitance variation with temperature, AC impedance measurements (in the frequency range of 10^6 to 10^{-2} Hz) of the electrode at different temperatures were conducted, and the results are displayed in Fig. 7. The Nyquist plot of impedance of the MnO_2 electrode consists of an arc and a spike. The arc at higher frequency region should be associated with the charge transfer process at electrode/electrolyte interface, and the spike at lower frequency region should be ascribed to the diffusion of Li^+ ions in MnO_2 solid. It can be seen from Fig. 7 that the ohmic resistance, charge transfer resistance and diffusion impedance all decrease with temperature increasing. The result suggests that a better kinetics of the electrode can be obtained at an elevated temperature, and this is consistent with the cyclic voltammetric result in Fig. 4. This should be responsible for the capacitance increase as temperature increased from 15 to 25 °C. However, it cannot explain the capacitance reduction as temperature further increased from 25 to 35 °C.

Fig. 8 shows the charge/discharge current efficiency of the MnO_2 electrode versus charge/discharge current rate at 25 and 35 °C. The current efficiency increases with current rate increasing either at 25 or at 35 °C. However, at any current rate, the

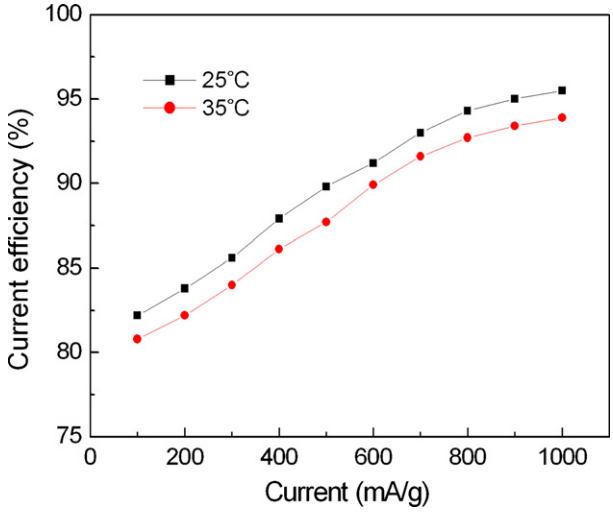

Fig. 8. Charge/discharge efficiency vs. current rate for the MnO_2 electrode at different temperatures.

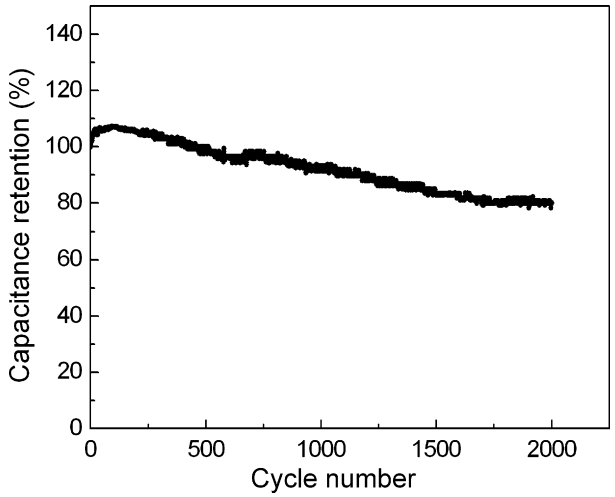

Fig. 9. Charge/discharge cycle life of the MnO_2 electrode at a current rate of 1000 mA g^{-1}.

current efficiency at 25 °C is higher than that at 35 °C. This may be explained as follows: in the charging process, the electrode potential increases gradually as charging proceeds. During the later stage of charging, the side reaction of oxygen evolution starts and competes with the primary oxidation reaction of the MnO_2 electrode itself. Temperature increment favors the side reaction of oxygen evolution (especially in the case of 35 °C, see Fig. 4) and hence decreases the charge/discharge current efficiency. Increase of temperature from 25 to 35 °C cannot only improve the reaction kinetics of the MnO_2 electrode itself, but also can facilitate the side reaction of oxygen evolution even more. This should be responsible for the capacitance reduction as temperature increased from 25 to 35 °C.

3.4. Cycle life of nanostructured manganese dioxide electrode

Fig. 9 shows the charge/discharge cycle life of the MnO_2 electrode operated in the potential range 0–1 V with a charge/discharge current rate of 1000 mA g^{-1} at 25 °C. It can be seen that in the initial 100 cycles, the discharge specific capacitance increases gradually. Hereafter, the specific capacitance begins to decrease. However, starting from the 1700th cycle, the specific capacitance seems no longer decreasing up to the 2000th cycle, and the capacitance retention is ca. 80% of the initial cycle. As far as metal oxide electrodes are concerned, the electrode exhibited a good cyclability at high charge/discharge current rate.

4. Conclusions

In this paper, the nanostructured manganese dioxide electrode material was prepared by sol–gel technique, and characterized by XRD and IR analysis as well as TEM observation. Experimental results demonstrated that temperature has a crucial influence on the discharge specific capacitance of the electrode. The specific capacitance obtained at different temperatures is in the following order: 25 °C > 35 °C > 15 °C. At the temperature of 25 °C, a high specific capacitance of 317 F g^{-1} can be obtained at a current rate of 100 mA g^{-1}, and a specific capacitance of 184 F g^{-1} can be obtained even at a high current rate of 1000 mA g^{-1}. The electrode exhibited good rate charge/discharge ability and cyclability at high current rate, and can be expected for use in manganese dioxide/activated carbon hybrid supercapacitors with lithium hydroxide electrolyte.

References

[1] W.G. Pell, B.E. Conway, W.A. Adams, J.D. Oliveira, J. Power Sources 80 (1999) 134.
[2] M. Endo, T. Maeda, T. Takeda, Y.J. Kim, K. Koshiba, H. Hara, M.S. Dresselhaus, J. Electrochem. Soc. 148 (2001) A910.
[3] J.P. Zheng, T.R. Jow, J. Power Sources 62 (1996) 155.
[4] K.W. Nam, W.S. Yoon, K.B. Kim, Electrochim. Acta 47 (2002) 3201.
[5] V. Srinivasan, J.W. Weidner, J. Power Sources 108 (2002) 15.
[6] Z.J. Lao, K. Konstantinov, Y. Tournaire, S.H. Ng, G.X. Wang, H.K. Liu, J. Power Sources 162 (2006) 1451.
[7] S.Y. Wang, K.C. Ho, S.L. Kuo, N.L. Wu, J. Electrochem. Soc. 153 (2006) A75.
[8] T.P. Gujar, V.R. Shinde, C.D. Lokhande, S.H. Han, J. Power Sources 161 (2006) 1479.
[9] K.R. Prasad, K. Koga, N. Miura, Chem. Mater. 16 (2004) 1845.
[10] K.R. Prasad, N. Miura, Electrochem. Commun. 6 (2004) 849.
[11] H.Y. Lee, J.B. Goodenough, J. Solid State Chem. 144 (1999) 220.
[12] S.C. Pang, M.A. Anderson, T.W. Chapman, J. Electrochem. Soc. 147 (2000) 444.
[13] M. Toupin, T. Brousse, D. Bélanger, Chem. Mater. 14 (2002) 3946.
[14] R.N. Reddy, R.G. Reddy, J. Power Sources 132 (2004) 315.
[15] K.R. Prasad, N. Miura, J. Power Sources 135 (2004) 354.
[16] Y.S. Chen, C.C. Hu, Y.T. Wu, J. Solid State Electrochem. 8 (2004) 467.
[17] M. Toupin, T. Brousse, D. Bélanger, Chem. Mater. 16 (2004) 3184.
[18] X. Wang, X. Wang, W. Huang, P.J. Sebastian, S. Gamboa, J. Power Sources 140 (2005) 211.
[19] V. Subramanian, H. Zhu, R. Vajtai, P.M. Ajayan, B. Wei, J. Phys. Chem. B 109 (2005) 20207.
[20] J.N. Broughton, M.J. Brett, Electrochim. Acta 50 (2005) 4814.
[21] Y. Chen, M.L. Zhang, Z.H. Shi, J. Electrochem. Soc. 152 (2005) A1272.
[22] S. Devaraj, N. Munichandraiah, Electrochem. Solid State Lett. 8 (2005) A373.
[23] K.W. Nam, K.B. Kim, J. Electrochem. Soc. 153 (2006) A81.
[24] S.L. Chou, F.Y. Cheng, J. Chen, J. Power Sources 162 (2006) 727.
[25] S.L. Kuo, N.L. Wu, J. Electrochem. Soc. 153 (2006) A1317.
[26] T. Brousse, M. Toupin, R. Dugas, L. Athouël, O. Crosnier, D. Bélanger, J. Electrochem. Soc. 153 (2006) A2171.
[27] S.E. Chun, S.I. Pyun, G.J. Lee, Electrochim. Acta 51 (2006) 6479.
[28] Anbao Yuan, Qinglin Zhang, Electrochem. Commun. 8 (2006) 1173.
[29] D.K. Walanda, G.A. Lawrance, S.W. Donne, J. Power Sources 139 (2005) 325.
[30] M.V. Ananth, S. Pethkar, K. Dakshinamurthi, J. Power Sources 75 (1998) 278.